Supporting information for: Plasmon assisted Nd^{3+} based solid-state nanolaser

Pablo Molina,[1] Eduardo Yraola,[1] Mariola O. Ramírez,[1] Christos Tserkezis,[2] José L. Plaza,[1] Javier Aizpurua,[2] Jorge Bravo-Abad[3] and Luisa E. Bausá[1]*

[1]Dept. Física de Materiales and Instituto Nicolás Cabrera, Universidad Autónoma de Madrid, 28049-Madrid, Spain

[2]Center for Materials Physics (CSIC-UPV/EHU) and Donostia International Physics Center (DIPC), Paseo Manuel Lardizabal 4, 20018-Donostia-San Sebastián, Spain

[3]Dept. Física Teórica de la Materia Condensada and Condensed Matter Physics Center (IFIMAC), Universidad Autónoma de Madrid, 28049-Madrid, Spain

Sample preparation

Nd^{3+}:PPLN laser crystal was grown by the off-centered Czochralski technique along the *x*-axis.[1] The period length was controlled via rotation and pulling rates (30 rpm and 1 mm/h, respectively) to generate a closely 50% duty cycle of alternating antiparallel ferroelectric domains with a periodicity close to 7 μm. The Nd^{3+} concentration was found to be 0.1 at % relative to Nb^{5+} as determined by total-reflection X-ray fluorescence.

The photoinduced silver deposition process was carried out by illuminating during 5 min an optical grade polished surface of a 0.8 mm thick *c*-cut Nd^{3+}:PPLN crystal with a UV Mercury pen-lamp (UVP model 11SC-1, its main line at 253.6 nm) while the sample was immersed in 0,01 M $AgNO_3$ solution at 70 ºC. The size and distribution of the silver NP chains were analyzed by means of scanning electron microscopy (SEM) using a Philips XL30 Schottky field emission gun electron microscope. The Ag NP chain length was around 2 mm and the separation between two chains was 3.5 μm. A representative high resolution SEM image showing the average interparticle distance (close to 2 nm) is displayed in Figure 1. Optical micrographs were obtained with an Olympus BX51 microscope equipped with crossed polarizers and a Nomarski modified Wollaston prism.

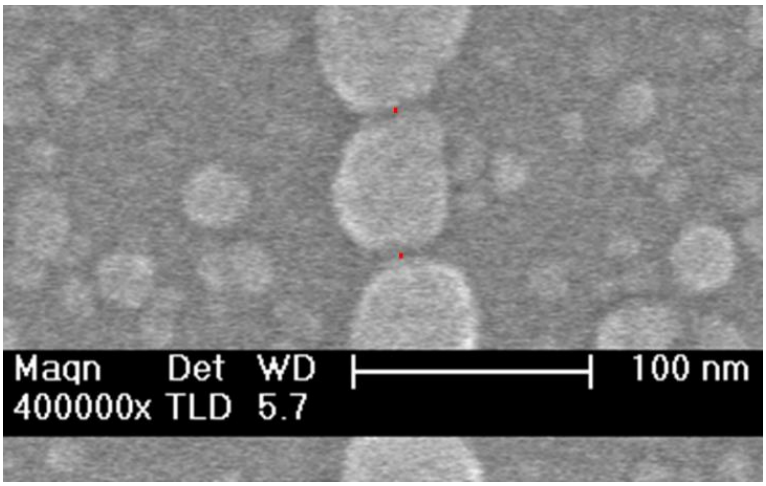

Figure 1: High resolution SEM image showing the NPs diameter and interspacing distance between adjacent NPs. The small red bars in between the NPs correspond to 2nm.

Laser experiments

For laser experiments, a *c*-cut 5 x 5 x 0,8 mm (L x W x T) Nd^{3+}:PPLN plate was placed inside a Fabry–Pérot resonator formed by two plane-parallel mirrors (M1 and M2). M1 was coated for high reflection (R>99.8 %) at the laser wavelength (λ_e=1093 nm) and for high transmittance (T>95%) at the pumping wavelength (λ_a=808 nm), while M2 was coated for high reflection for both, the pump (R>99.8 %) and laser (R>97 %) wavelengths. The mirrors were separated at their edges by two 1 mm thick spacers to avoid the direct contact with the surface of the sample. Assuming that the only source of losses arises from the partial reflectance of the mirrors, the quality factor of the mirror cavity can be estimated as:[2]

$$Q = \frac{\nu_0}{\nu_f} F = \frac{\nu_0}{\nu_f} \frac{\pi\sqrt{\Re}}{(1-\Re)} \qquad (1)$$

where ν_0 corresponds to the resonant frequency (ν_0 = 9149 cm^{-1}), ν_f is the spacing between longitudinal modes, $\nu_f = c/2d$, and F is the finesse of the resonator defined by $F = \pi\sqrt{\Re}/(1-\Re)$ where $\Re$ refers to the mirror reflectance ($\Re \approx R_1 R_2$)$^{1/2}$. Thus, in

our particular case, the upper limit for the quality factor of the mirror cavity can be set at $Q = 3.5 \cdot 10^5$. However, a more accurate estimation should consider the internal cavity losses, in particular, those associated with the gain medium (absorption, scattering,...etc). To account for these effects, the quality factor Q for the conventional bulk laser operation was estimated from the experimental results according to the expression:[2]

$$Q = \frac{\nu_0}{\delta\nu} \tag{2}$$

where $\delta\nu$ corresponds to spectral linewidth of a single longitudinal mode (full width at half maximum (FWHM) of the resonant peak). In our experiments, the stimulated emission for the bulk Nd^{3+}:$LiNbO_3$ solid state laser takes place at λ_e=1093 nm (ν_0 =9149 cm^{-1}). The measured spectral linewidth was found to be: $\delta\nu$=0.8 cm^{-1}, which leads to a quality factor value of $Q = 1.14 \cdot 10^4$. This relatively low value is related to the large losses caused by the bulk photorefractive damage of $LiNbO_3$.[3]

The whole system was positioned on a customized scanning confocal microscope (Olympus BX41) provided with a two-axis XY motorized platform (0.2 μm spatial resolution) driven by Labspec software. As excitation source we used a cw Ti:sapphire laser (Spectra Physics) tuned at 808 nm. An objective lens, 20x with a numerical aperture (NA) = 0.45, was used to focus the pump beam to a 2.2 μm-diameter spot onto the sample. The laser spectra were collected in backscattering geometry with the same objective, and directed by an optical fiber to a Peltier-cooled Horiba Synapse CCD attached to a Horiba iHR 550 monocromator. The polarization of the pump laser beam was selected by means of a $\lambda/2$ plate. The input-output laser curves were also obtained in confocal geometry recording two dimensional spatial maps by integrating the laser intensity for different values of the pump power. All the experiments were carried out at room temperature.

Numerical calculations

Full-wave three-dimensional (3D) simulations of the considered chain of silver metallic NPs lying on top of a laser crystal were performed using both a finite-difference time-domain (FDTD) approach (Lumerical Inc.) and a finite-element method (FEM; COMSOL Multiphysics package). Open space in both types of simulations was mimicked by using perfectly matched layers or/and scattering boundary conditions. Periodic boundary conditions were used to simulate the optical response of an infinitely periodic chain of metallic NPs. The dielectric permittivity of silver metallic NPs was modeled following Ref. 4. A Sellmeier formula was used to model the refractive index of the laser crystal.[5] The discretization grids in the simulations were refined until a relative numerical error of less than 1% is achieved in all reported results. No additional approximations, apart from the one introduced by the spatial discretization of the dielectric constant (inherent to any FDTD or FEM implementation) were introduced in the simulations, and no fitting parameters to the experimental data were assumed in the calculations.

Semi-analytical laser model

We used a semi-analytical theoretical approach based on a simple formulation of the Maxwell-Bloch equations.[6,7] This model allows us to obtain compact expressions of the main lasing characteristics of the system in terms of a small number of effective parameters (which, in turn, can be obtained from the full-wave simulations described above). Specifically, assuming a conventional four-level description of the emitters forming the lasing medium and solving for steady-state photon- and electron-population numbers, we obtained the following analytical expressions for the lasing threshold (R_p^{th}) and slope efficiency (G_e), $R_p^{th} = V_a / (Q_e \Gamma \zeta)$ and $G_e = Q_e / \omega_e$. Here V_a is the volume of

the laser medium and Q_e is the quality factor of the plasmonic resonance. Γ represents the energy confinement factor at the lasing frequency, $\Gamma = \int_{V_a} d\mathbf{r}\, u(\mathbf{r},t) / \int dr\, u(\mathbf{r},t)$ (with $u(\mathbf{r},t)$ being the time-average over one optical period of the density of electromagnetic energy). The parameter ζ is defined as $\zeta = v_g \sigma_e \tau_{21} N_0 / \omega_e$, where v_g is the material group velocity of the active medium, σ_e (5 x 10^{-20} cm^2) is the emission cross-section of the laser emitters, N_0 is the total number of emitters, and τ_{21} (100 μs) is the spontaneous emission lifetime of the considered laser transition.

Extent of improvement of the laser threshold for the plasmon-assisted geometry

We have estimated the variation of threshold for the plasmonic system when considering different NA values, i.e. different spot sizes on the surface of the crystal. Since the Ag NP chain length on the surface of the SSL crystal was around 2 mm, varying the magnification of the objective will result in the participation of different number of NPs on the lasing process. Taking into account that different spot sizes illuminate different number of Ag NPs, we have calculated the scattering cross-section values (σ_N) at the pump wavelength (λ_a=808 nm) for chains formed by different number (N) of interacting Ag NPs, with values of N ranging from N=15 to N=50. The calculations have been performed by solving Maxwell's equations with the use of the boundary-element method (BEM).[8,9] In these calculations we have considered spherical Ag NPs with an average size of 50 nm and interspacing distances of 2 nm forming linear chains. The results are shown in Fig. 2a, together with the scattering cross-section values per NP (σ_N/N) as a function of N (Fig. 2b). It should be mentioned that increasing the number of interacting NPs above N= 15 does not significantly change the spectral shape of the scattering cross-

section spectrum, but only its intensity. In contrast, the spectral shape of the short chain modes (*N* in the range 1-15) strongly varies with the number of particles, displaying, additionally, a weaker radiative nature.[10] That is the reason why we have considered *N* from 15 to 50 in our analysis. Note that NA= 1.4 (limit case) and NA= 0.45 correspond to illuminating 15 and 45 NPs, respectively (see Table 1)

As observed in Fig. 2b, the scattering-cross section per NP (σ_N/N) depends on the illuminated area (that is, on the number of illuminated particles *N*). Accordingly, the smaller σ_N/N, the higher pump power density needed to achieve similar population inversion of Nd^{3+} ions. For the 100x objective (NA = 1.4), the pump power density at threshold has been estimated by correcting the experimentally obtained value for a 20x objective by a ($\sigma_{45}/45$)/($\sigma_{15}/15$) factor, which is equal to 1.3.

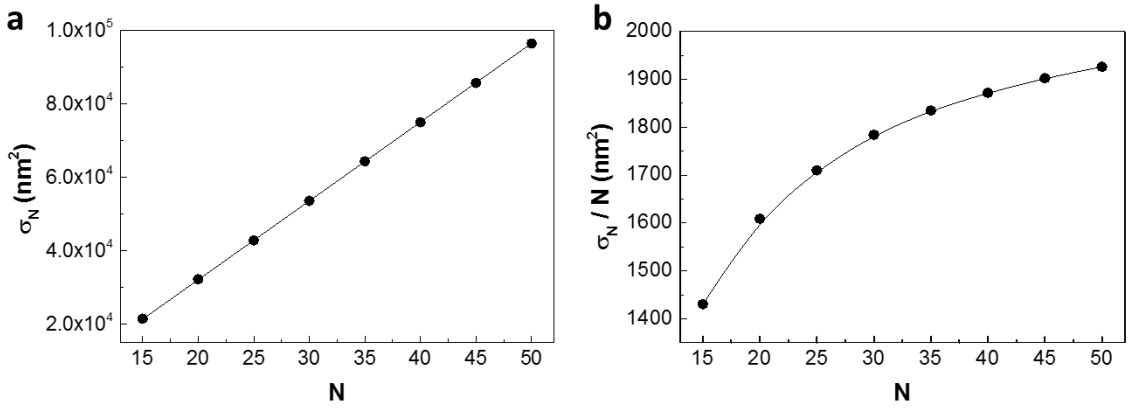

Figure 2: (a) Calculated scattering cross section of chains with different number of NPs as a function of the number of particles *N*; (b) Calculated scattering cross section per NP vs *N*.

Regarding the case of conventional laser action from the bulk crystal (without plasmonic nanostructures), modifying the NA affects the laser cavity conditions in an involved way. In addition to the variations of the pump power density on the surface of the laser crystal, varying NA also affects the modal volume via the confocal parameter and the pump beam divergence inside the cavity. These factors dramatically influence the laser performance

of the bulk crystal. In fact, increasing NA from a conventional 20x objective to a 100x objective could even result into an increase of the pump power at threshold for the solid state laser.Consequently, the plasmonic effect is going to be clearly evidenced for the extreme case of a minimum number of illuminated particles of 15, which corresponds to the limit of focalization with an oil inmersion 100x objective (NA=1.40). Finally, we think that one of the advantage of our system lies in the fact that it is possible to get threshold conditions for laser action in a nanometric spatial region without the need of a tight focusing.

Table 1: Estimation of the threshold variation for the plasmonic system for two different NA

Objective	Pump spot area ($x\ 10^5\ nm^2$)	Illuminated particles (N)	σ_N at 800nm (nm^2)	σ_N/N (nm^2)	Power density at threshold (mW/nm^2)	Pump power at threshold (mW)
20x (NA =0.45)	38	45	8.5×10^4	1.89×10^3	3.3×10^{-5} (experimental)	**125 (experimental)**
100x (NA =1.40)	3.9	15	2.15×10^4	1.43×10^3	4.3×10^{-5}	**16.7**

REFERENCES

(1) Ming, N. B.; Hong, J. F.; Feng D. *J. Mater. Sci.* **1982**, 17, 1663-1670.

(2) Bahaa E. A., Saleh, Malvin C. T. *Fundamentals of Photonics*; John Wiley & Sons, Inc, New York, 1991.

(3) Fan, T. Y.; Cordova-Plaza, A.; Digonnet, M. J. F.; Byer, R. L.; Shaw, H. J. *J. Opt. Soc. Am. B* **1986**, 3, 140-148

(4) Johnson, P. B.; Christy, R. W. *Phys. Rev. B* **1972**, 6, 4370-4379.

(5) Zelmon, D.E.; Small, D.L.; Jundt, D. *J. Opt. Soc. Am. B* **1997**, 14, 3319–3322.

(6) Chang, S. W.; Chuang, S. L. *IEEE J. Quantum Electron.* **2009**, 45, 1004-1013.

(7) Cuerda, J.; Ruting, F.; Garcia-Vidal, F. J.; Bravo-Abad, J. *Phys. Rev. B* **2015**, 91, 041118(R).

(8) García de Abajo, F. J.; Aizpurua, J. *Phys. Rev. B* **1997**, 56, 15873.

(9) García de Abajo, F.J.; Howie, A. *Phys. Rev. B* **2002**, 65, 115418.

(10) Yraola, E.; Sanchez-Garcia, L.; Tserkezis, C.; Molina, P.; Ramirez, M. O.; Plaza, J. L.; Aizpurua, J.; Bausa, L. E. *Opt. Exp.* **2015**, 23, 15672.